*Computer Methods in Biomechanics and Biomedical Engineering*

**Preprint**

# Validation of Composite Finite Elements Efficiently Simulating Elasticity of Trabecular Bone

Lars Ole Schwen[a] and Uwe Wolfram[b,c*]

[a] *Fraunhofer MEVIS, Bremen, Germany*
[b] *Institute of Orthopaedic Research and Biomechanics, Ulm University, Ulm, Germany*
[c] *Present Address: Institute for Surgical Technology and Biomechanics, University of Bern, Bern, Switzerland*

Patient specific analyses of the mechanical properties of bones become increasingly important for the management of patients with osteoporosis. The potential of Composite Finite Elements (CFEs), a novel FE technique, to assess the apparent stiffness of vertebral trabecular bone is investigated in this study.

Segmented volumes of cylindrical specimens of trabecular bone are compared to measured volumes. Elasticity under uniaxial loading conditions is simulated, apparent stiffnesses are compared to experimentally determined values. Computational efficiency is assessed and recommendations for simulation parameters are given.

Validating apparent stiffnesses results in concordance correlation coefficients $0.69 \leq r_c \leq 0.92$ for resolutions finer than 168 µm and an average error of 5.8 % between experimental and numerical results at 24 µm resolution.

To show the potential, the code was used to compute local, macroscopic stiffness tensors for the trabecular structure of a lumbar vertebra (L4).

The presented technique allows for computing stiffness using smooth FE meshes at resolutions that are well achievable in peripheral high resolution quantitative CTs. Therefore, CFEs could be a valuable tool for the patient-specific assessment of bone stiffness.

**Keywords:** apparent stiffness; composite finite elements; linearised elasticity; nanoindentation; trabecular bone; validation

## 1. Introduction

Osteoporosis-related fractures represent a major public health problem. Predicting fracture load from high resolution CT datasets could be very useful for osteoporosis management. It was shown that fracture load can be predicted with large scale µFE models based on µCT datasets (Pistoia et al. 2002). Such an approach necessitates efficient algorithms to setup reliable µFE models and compute the fracture load of the structure of interest.

To investigate mechanical properties of trabecular bone *in silico*, voxel-based µFE models are usually used (Faulkner et al. 1991; Müller et al. 1994; Guo and Kim 2002; van Rietbergen et al. 2003; Morgan et al. 2005; Thurner et al. 2006; Woo et al. 2007; Chevalier et al. 2007). Disadvantages of those models are the nonsmooth meshes and their dependence on high resolutions (Verhulp et al. 2008; Wolfram et al. 2010). Smoothing of meshes obtained directly from µCT voxel data (Boyd and Müller 2006) can remedy non-smoothness in the surface representation but may lead to distorted

*Corresponding author. Email: uwe.wolfram@istb.unibe.ch, Phone: +41 31 631 5926, Institute for Surgical Technology and Biomechanics, Stauffacherstrasse 78, CH-3014 Bern, Switzerland

ISSN: 1741-5977 print/ISSN 1741-5985 online

DOI: 10.1080/1741597YYxxxxxxxx
http://www.informaworld.com

elements. Tetrahedrisations of the scanned objects suitable for FE simulations are not obtained trivially (Bern and Eppstein 1992; Teng and Wong 2000; Shewchuk 2002). Furthermore, computational efficiency suffers from their inherently unstructured nature.

In classical µFE models, the geometric complexity of trabeculae is represented in the mesh. To overcome the aforementioned disadvantages in classical µFE models, composite finite elements (CFEs) were introduced (Hackbusch and Sauter 1997a,b, 1998). Their key property is that they use the hexahedral mesh given immediately by the voxel image data and represent the geometric shape with sub-pixel accuracy in adapted basis functions (Liehr et al. 2009; Schwen 2010).

As any computational method, CFEs should be validated against *in vitro* experiments before they can be used in biomechanical analyses. Therefore, the goals of this study are 1) to validate the segmentation approach used for the CFE construction; 2) to validate the CFE simulation of uniaxial compression and tension experiments using linearised elasticity; and 3) to assess computational efficiency and to determine simulation parameters such as imaging resolution and solver accuracy. As a final application, we show simulation and numerical homogenisation results obtained for the trabecular core of a lumbar vertebra.

## 2. Materials and Methods

### *2.1 Volume Measurement*

For the validation of the segmentation approach, six bovine (age between 6 and 9 months), six porcine (age between 6 and 9 months), six young ♂ human (37 y) and six old ♀ human (92 y) cylindrical trabecular bone specimens of $8 \times 12$ mm were obtained from vertebrae of the thoraco-lumbar region. The endplates of the vertebrae were removed using a high precision band saw (Exakt Apparatebau, Norderstedt, Germany). The cylinders were cored from the remaining vertebral plates using a dental trepan (229XL 080, Hager & Meisinger, Neuss, Germany) and freed from marrow using a pulsed water-jet (Braun Oral-B Professional Care 6500, Kronberg, Germany). Thereafter, the cylinders were scanned in a µCT (XCT FAN Beam µ-Scope, Stratec Medizintechnik GmbH, Pforzheim, Germany) at a spatial resolution of 30 µm.

Sample volume was experimentally measured using a gas micro-pycnometer (helium gas micro-pycnometer, AccuPyc 1330, Micromeritics, Norcross, USA). Samples were submerged in helium and the volume was determined from the ousted gas volume. *In silico*, the volumes were determined from the reconstructed and thresholded CT dataset by a) counting voxels or b) determining the interior in the CFE construction described below. The threshold needed for both these was determined according to (Ridler and Calvard 1978). This threshold, which in general is not integer-valued, is later referred to as $\tau$.

To later investigate the dependence of the apparent mechanical properties on the image resolution, µCT datasets were coarsened by an integer factor $c$. Coarsening was performed by averaging blocks of $c^3$ voxels of the original scan, possibly dropping excess slices at the boundary. The threshold previously determined for the finest resolution was used for all downsampled resolutions.

### *2.2 Mechanical Tension and* In Vitro *Compression Tests*

For the validation of the CFE-method against mechanical tests, experimental data from a previous validation study (Wolfram et al. 2010) were used. Briefly, the material

consisted of 16 fresh frozen vertebrae (T6 to L2; 7 ♂, 3 ♀ donors) with a median age of 51 y (range: 37 to 84 y). After preparation, 20 cylindrical samples with 8 mm diameter and, depending on the vertebral height, 18 to 25 mm height were cored from the vertebra and endcapped so that an approximately 12 mm free gage length was obtained. The cylinders were scanned in a different µCT (µCT 40, SCANCO Medical AG, Brüttisellen, Switzerland) at a spatial resolution of 12 µm. The scanner software provides a segmentation threshold for the specimens considered here by a method similar to the one (Ridler and Calvard 1978) used above. Voxel-based and CFE-based volumes were determined as before.

Prior to apparent testing, cylindrical samples were rehydrated in 0.9 % physiological buffered solution. Aluminium rods were attached to the endcaps using cyanoacrylate and an extensometer was applied to the PU endcaps spanning the free testing length after mounting the specimen on the testing system (Mini-Bionix MTS system, Milwaukee, MN, USA). Testing was performed under moist conditions. The samples were (mechanically) preconditioned with three cycles to $\varepsilon = 0.4\,\%$ strain at a strain rate of $\dot{\varepsilon} = 0.4\,\%\mathrm{s}^{-1}$. Subsequently, the specimens were loaded up to $\varepsilon = 0.004$ strain at a strain rate of $\dot{\varepsilon} = 0.2\,\%\mathrm{s}^{-1}$ (Wolfram et al. 2010). Stresses were calculated from the force and strain curves by dividing the obtained forces by the initial cross section area of the bounding cylinder.

### *2.3 Tissue Material Parameters*

Tissue material parameters for the samples designated for mechanical testing were obtained from the surrounding tissue using nanoindentation (Wolfram et al. 2010). After coring the cylinders, a 5 mm thick trabecular slice was obtained from the surrounding trabecular tissue using a high precision band saw (Exakt Apparatebau, Norderstedt, Germany). Subsequently, a mild preparation protocol was applied to conserve tissue mechanical properties (Wolfram et al. 2010). After curing, the samples were embedded in epoxy resin (Struers A/S, Ballerup, Denmark), polished with increasing grades of silicon carbide paper (P1000, P1400, P2000, P2500, P4000 – Hermes Schleifmittel GmbH & Co. KG, Hamburg, Germany) and finished with 1 µm diamond paste on a polishing cloth. Prior to testing, the samples were rehydrated in 99% saturated Hank's Balanced Salt Solution (HBSS) for 1.5 h. Indentations were performed on samples submerged in HBSS using a pyramidal Berkovich diamond tip mounted in a depth-sensing nanohardness tester additionally equipped with a wet cell (CSM Instruments SA, Peseux, Switzerland). Indentations were driven to 2.5 µm depth at $0.002\,\mathrm{Ns}^{-1}$. Load was maintained for 30 s to prevent creep influences. Subsequently, the samples were unloaded at $0.002\,\mathrm{Ns}^{-1}$. Six indentations were performed on three axial trabecular cross-sections providing 18 indentation measurements per cylindrical specimen. A Poisson's ratio of 0.32 was assumed for the bone tissue (Rho et al. 1997; Hengsberger et al. 2003). Tissue elastic moduli were determined (Oliver and Pharr 1992) and averaged over all 18 indentations per sample.

### *2.4 Composite Finite Element Simulations*

CFEs use a level set representation (Osher and Sethian 1988) of the object of interest. This is obtained from the µCT voxel image $g$ using the thresholds $\tau$ described above using the affine transformation of the grey values $g_\tau = -g + \tau$. The trabecular structure is then represented by $[g_\tau < 0]$, i.e. trabecular bone corresponds to negative values of $g_\tau$ and the zero isosurface of $g_\tau$ represents the bone pore interface. It has to be mentioned that this transformation of grey values is compatible with (and actually commutes with) the resampling described above. Figure 1 shows the CFE

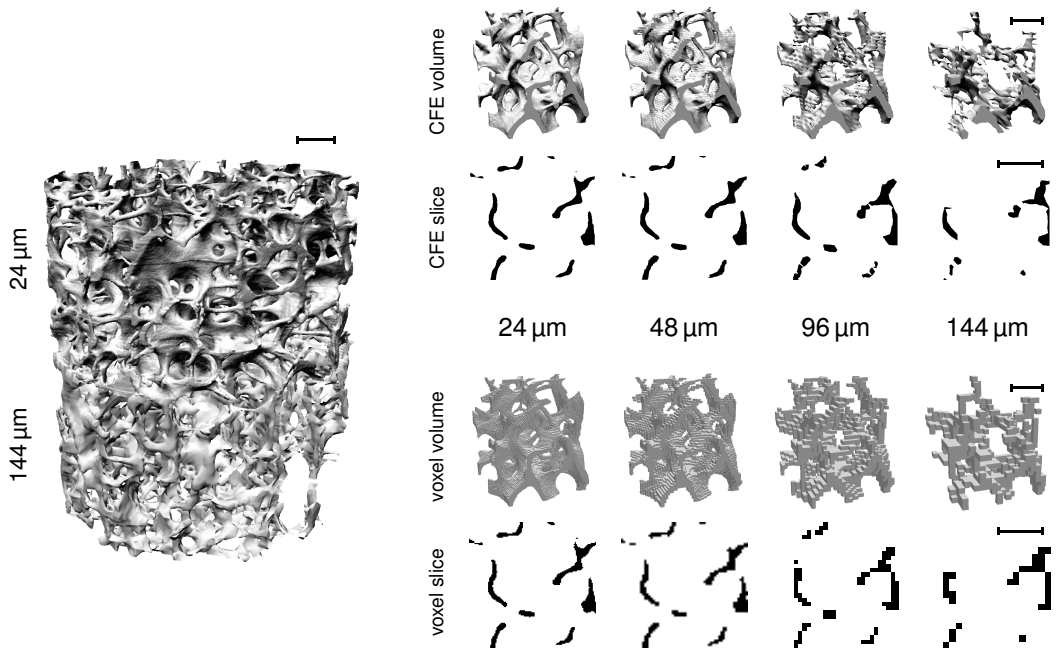


**Figure 1:** On the *left*, the CFE interface of one human trabecular specimen used in our simulations is shown at resolution 24 µm *(upper half)* and 144 µm *(lower half)*. On the *right*, a small subset of the specimen is considered. The shape of the object and one slice in the CFE representation is shown for decreasing µCT resolution. For comparison, the corresponding voxel-based volumes and slices are shown below. Notice that, at fixed resolution, the CFE and voxel-based simulations use the same set of degrees of freedom associated to the hexahedral (voxel) computational mesh. The CFEs, via sub-pixel adaption of basis functions, are capable of capturing more geometric detail as the voxel size approaches the trabecular thickness. Black bars corresponding to 1 mm length indicate the different scales in the visualisation.

representation of one of the cylindrical specimens and the influence of the imaging resolution on the geometric accuracy of the CFE representation compared to a voxel-based model.

The CFE construction for complicated domains (Liehr et al. 2009; Schwen 2010) basically works as follows. Each hexahedron in the grid defined by voxel midpoints is subdivided in six tetrahedra in such a way that edges on the faces of neighbouring cubes coincide. Finding the zero crossings of the level set function on these tetrahedral edges (by affine interpolation) allows restricting standard affine-linear FE basis functions on the tetrahedra to the approximate interior. Hence, no additional DOF are introduced except for those associated to vertices in the hexahedral voxel grid.

A standard conjugate gradient solver using SSOR (numerical) preconditioning (Hackbusch 1994) was used for solving the systems of equations arising from this type of simulation, as indicated by a solver performance comparison in (Schwen 2010).

Tension or compression by 0.1 mm was simulated assuming isotropic, linearised elasticity of the trabecular tissue with the parameters as described above. The corresponding force was subsequently evaluated and the apparent elastic moduli were determined (Wolfram et al. 2009).

### *2.5 Statistical Analysis*

Statistical analyses were performed with R (R Development Core Team 2008). The agreement between experiment and simulation with respect to the volume measurements and apparent stiffness was evaluated with concordance correlation

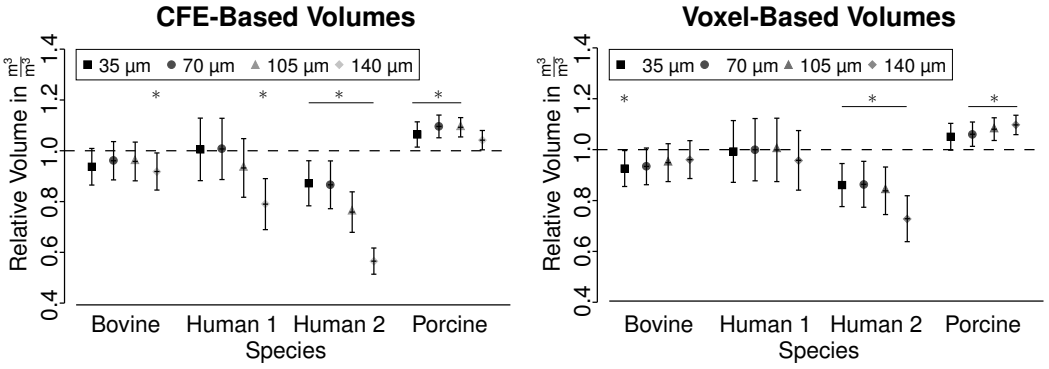


**Figure 2:** Volume segmentation depending on the image resolution. The relative volume was computed by dividing the volume determined *in silico* by the experimentally measured volume. The black horizontal line and the asterisk indicate relative volumes significantly different from one, which would indicate specimen wise concordance with the experimental data.

coefficients $r_c$ (Lin 1989). The models were considered valid if $r_c > 0.90$. Due to linear quantile-quantile plots the $t$-test was used to compare groups applying a significance level of $p < 0.05$.

### *2.6 Application: Numerical Homogenisation in the Vertebral Core*

As an application example, local stiffness tensors are computed for the trabecular core of a ♀ human lumbar vertebra (58 y). The posterior structures were removed using a band saw. The vertebra was wrapped in foil and scanned in a µCT (Skyscan 1172, Skyscan, Kontich, Belgium) at a spatial resolution of 30 µm.

From the scan, a slice of 21 mm thickness was selected and resampled by a factor of 3, resulting in 90 µm image resolution. By the same procedure as before, the vertebral slice was used in a compression simulation by 0.1 mm, assuming isotropic elasticity properties with $E = 13$ GPa and $\nu = 0.32$. Moreover, 59 cubes of 6 mm edge length ($200^3$ voxels) of the vertebral core were selected, smoothed using Gaussian smoothing ($\sigma = 2$ voxels) and resampled to resolution $150^3$ using multilinear interpolation. For these subsets of the trabecular bone, effective elasticity properties were determined numerically by a method described previously (Rumpf et al. 2010). In summary, deformations by elementary displacements are simulated and the respective stresses are evaluated on an interior subdomain (to avoid boundary stiffening artifacts) so that the effective elasticity tensor is determined. Microscopic material isotropy combined with geometric anisotropy then results in anisotropic effective material properties.

## 3. Results

### *3.1 Validation of Segmented Volumes*

The segmentation of the volumes indicates for small resolutions a better volume determination of the CFE approach in comparison to the voxel-based determination of the volumes (Figure 2). Both the CFE-based and voxel-based approach underestimated the bone volume of the elderly female donor. In contrast, both methods overestimated the volume of the porcine specimens. In case of the bovine specimens and the specimens of the young human donor, the CFE-based volume determination was able to detect the volume correctly for resolutions smaller than 140 µm. This was not reproduced by the voxel-based volume determination.

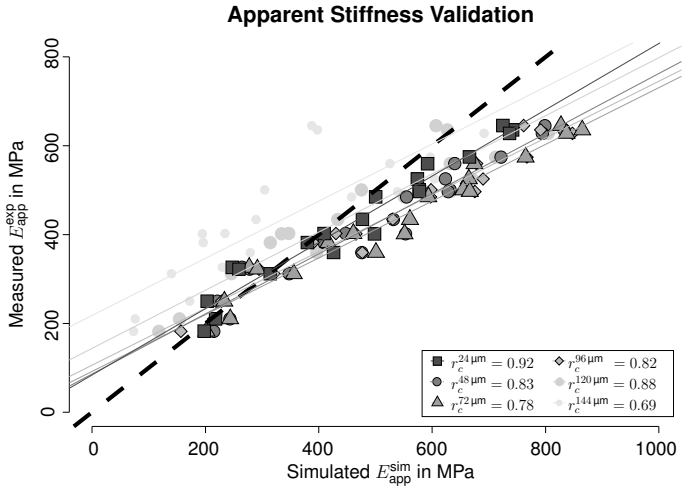


**Figure 3:** Concordance correlation straights for resolutions below 168 µm were statistically significant ($p < 0.05$) and indicate a moderate but acceptable concordance between experiment and simulation (apparent stiffnesses $E_{\text{app}}^{\text{exp}}$ and $E_{\text{app}}^{\text{sim}}$, respectively). Ideal concordance would have been given by a correlation straight falling together with the black, dashed line.

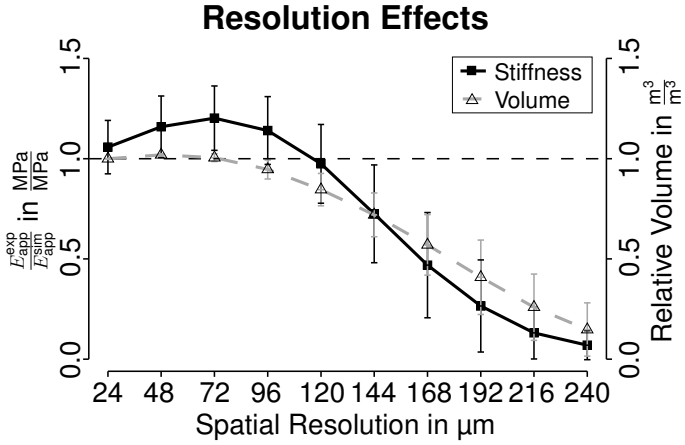


**Figure 4:** Relative apparent stiffness (computed stiffness $E_{\text{app}}^{\text{sim}}$ divided by experimentally determined stiffness $E_{\text{app}}^{\text{exp}}$) indicates that resolutions up to 120 µm allow to correctly determine mean apparent stiffnesses. Relative volumes (current volume divided by the volume calculated on the finest resolution) show a different evolution with resolution than relative apparent stiffness.

### *3.2 Validation of Apparent Stiffnesses*

The comparison of the compression and tension experiments with the respective simulation yielded concordance correlation coefficients of $r_c < 0.9$ but $r_c \geq 0.78$ for resolutions below 168 µm (Figure 3). The best concordance was achieved for a resolution of 120 µm. Interestingly, this was slightly smaller than the 140 µm that were the boundary for accurate prediction of the volume (Section 3.1). Nevertheless, the concordance correlation coefficients were all smaller 0.95. Thus, CFE-models did not deliver valid results comparing experiments and simulations in a one-to-one fashion.

The inclination fashion of the concordance straights (Figure 3) indicates that CFEs are at least well capable of providing correct mean results. This is further corroborated by comparing the mean relative apparent stiffness (Figure 4). Here a slight overestimation was found for resolutions {24, 48, 72, 96, 120} µm. At the same resolutions the relative volume of the samples did not change significantly.

**Table 1:** For one compression case and one tension case, the table shows the computational workload (wall clock time) of the system solver and resulting effective force $F_{\text{eff}}$ for different solver thresholds $\epsilon_{\text{tol}}$.

| | compression case | | | tension case | | |
|---|---|---|---|---|---|---|
| $\epsilon_{\text{tol}}$ | # iter | $F_{\text{eff}}$ in N | time in s | # iter | $F_{\text{eff}}$ in N | time in s |
| $10^{-2}$ | 32 | 119.474 | 82.4 | 31 | 10.726 | 68.0 |
| $10^{-3}$ | 185 | 190.755 | 513.1 | 189 | 133.462 | 408.3 |
| $10^{-4}$ | 589 | 188.338 | 1512.2 | 686 | 128.096 | 1592.7 |
| $10^{-5}$ | 939 | 188.125 | 2056.9 | 1137 | 127.971 | 2580.5 |
| $10^{-6}$ | 1573 | 188.147 | 3303.0 | 2231 | 127.959 | 4553.3 |
| $10^{-7}$ | 2282 | 188.149 | 5076.1 | 2735 | 127.958 | 5599.3 |
| $10^{-8}$ | 2889 | 188.149 | 6140.3 | 3587 | 127.958 | 7139.3 |

**Table 2:** For one compression case and one tension case, computational parameters (number of degrees of freedom, iterations of the system solver and its wall clock time duration) for simulations at different image resolutions are shown.

| | compression case | | | tension case | | |
|---|---|---|---|---|---|---|
| resolution | # DOF | # iter | time in s | # DOF | # iter | time in s |
| 48 µm | $3 \times 957\,370$ | 1573 | 3303.0 | $3 \times 734\,963$ | 2231 | 4553.3 |
| 72 µm | $3 \times 360\,093$ | 956 | 658.2 | $3 \times 269\,857$ | 1231 | 815.0 |
| 96 µm | $3 \times 177\,282$ | 1132 | 374.9 | $3 \times 133\,618$ | 1129 | 340.8 |
| 120 µm | $3 \times 99\,265$ | 1217 | 206.9 | $3 \times 75\,380$ | 1088 | 170.2 |

### *3.3 Computational Performance*

To assess the computational performance of the CFE method described, the system solver accuracy needed for robust results was investigated first. The results in Table 1 (for one of the compression and tension simulations, respectively) indicate that a stopping criterion of reduction of the residuum norm by six orders of magnitude is sufficient for computing the apparent stiffness in a robust manner. In the implementation (C++ code compiled with gcc 4.5.2 on Ubuntu 10.04, using OpenMP for some simple parallelisation and allowing up to four threads), 5 995 and 5 189 MiB of memory were needed and the simulations took about 55 and 76 minutes, respectively, on a 2.8 GHz Intel Core i7 CPU using IEEE double floating point accuracy, averaging 2.29 and 2.36 threads. For the simulations at 24 µm resolution, a compute server was necessary due to larger memory requirements.

Table 2 shows, for the solver accuracy described above, to what extent problem sizes and computational workloads decrease for coarser image resolutions of the same datasets and loading cases as before.

### *3.4 Simulation on a Whole Vertebra*

The result of the compression simulation on an almost complete vertebra ($608 \times 487 \times 233$ computational grid) is shown in Figure 5. The force corresponding to a compression of the object by 0.1 mm is 17 688.5 N.

Figure 5 moreover shows the the resulting effective elasticity tensors on different cubic subsets of the vertebral dataset. These were visualized (at the respective location inside the vertebra) as deformed and colored spheres according to (He and Curnier 1995; Cazzani and Rovati 2003) so that elongation encodes uniaxial compressive stiffness and color encodes the bulk modulus.

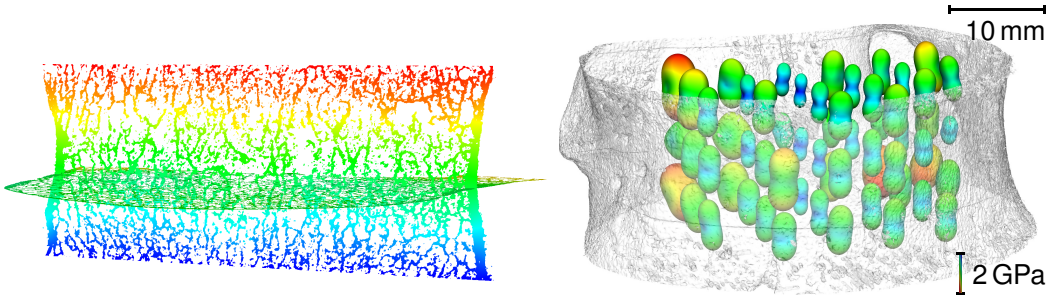


**Figure 5:** The *left* image shows the deformations obtained on two slices through a dataset of a vertebra subject to compression, color-coded from blue to red (maximum downward displacement). On the *right*, effective elasticity tensors obtained by numerical homogenisation on cubic subspecimens of the same vertebra are visualized. This shows both the anisotropy induced by the geometric microstructure and the inhomogeneity of macroscopic elasticiy properties.

## 4. Discussion

The paper is concerned with the validation and application of a promising FE-tool that allows to directly set up sooth µFE models of complicated domains such as trabecular bone. First, it is possible to accurately segment given volumes using an established segmentation technique and a CFE volume mesh. Second, CFEs allow to predict the apparent modulus of elasticity with a moderate but acceptable concordance coefficient. Third, computational efficiency was assessed to show that µFE-models of trabecular bone where usually compute servers are employed can be solved on a desktop PC using CFEs. In our case approximately one hour.

The volume measurements for the evaluation of the capabilities of the segmentation technique used for setting up the CFE-models could only be performed at a comparable coarse resolution of 35 µm. This due to the fact that no better µCT-scanner was available at that time. Different species with distinct bone morphology were selected to be able to test the segmentation on different measurement targets and because of a better availability of animal material. The good volume prediction in case of the bovine and young human specimens indicate that the resolution of the scanner was sufficient for these measurements. However, in case of the elderly female donor, low bone volume fraction and trabecular thickness could have led to partial volume effects which could have influenced the volume measurements. Parts of the volume could have been systematically segmented as background which led to the underestimation of the volume. The slight overestimation in case of the porcine samples could have been due to the higher bone volume fraction and the lower trabecular spacing. The indifferent volume prediction in case of the voxel-based volume determination may be an artifact caused by the non-smooth nature of the bone surface. Both the CFE-based and the voxel-based volume measurements showed only small errors at resolutions up to 105 µm in comparison to the experimental gas micro-pycnometer measurements. This experimental method was considered as gold standard since its measurement error is several orders of magnitude smaller than that of the used CT. Besides the resolution of the µCT, the segmentation technique (Ridler and Calvard 1978) used could have been a further source of error to these measurements. The advantage of the single-level threshold is its capability to provide an optimal threshold in an iterative procedure. This should ensure the best possible volume segmentation. For voxel-based µFE-models it is known that their capabilities to predict stiffness decreases dramatically with resolutions greater 60 µm (Verhulp et al. 2008; Bevill and Keaveny 2009) due to their non-smoothness. In providing an equally good volume segmentation CFEs could be a candidate to circumvent this disadvantage.

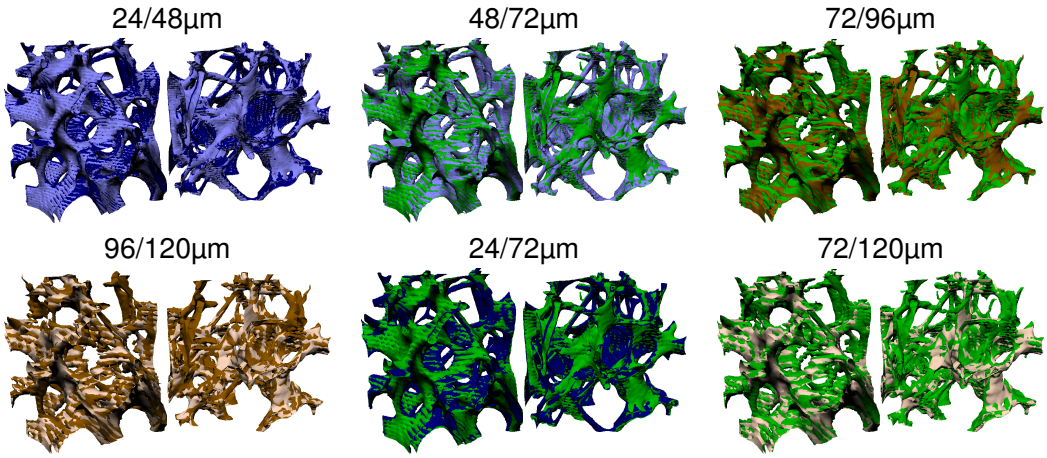


**Figure 6:** CFE models at different resolutions, front and back view of the same substructures each. Stiffer structures such as plates or junctions could have been over-segmented with increasing resolutions. At the same time more compliant structures such as rods could have been under-segmented. This could have led to the diverging evolutions of stiffness and volume (Figure 4). The effect seems to reverse at 72 µm. Dark blue denotes the interface at 24 µm, light blue at 48 µm, green at 72 µm, brown at 96 µm and light brown at 120 µm.

The stiffnesses determined *in silico* using CFEs correspond on average to those determined *in vitro*. The comparison in a one-to-one fashion delivered moderate but acceptable concordance to the *in vitro* measurements. However, compared to a similar study (Wolfram et al. 2010) that employed an already existing µFE-code (Arbenz et al. 2008) on the same samples, $r_c$ and, thus, the one-to-one concordance between simulation and experiment was approximately 10 % worse. Since the same threshold was used on the same datasets at similar resolutions this disagreement could be due to the nature of the CFEs or their implementation.

It was observed that different resolutions lead to larger differences in stiffness than the corresponding volume changes suggest (Figure 4). This could have been due to over- or underestimation of local volume elements such as plates and rods. CFE model generation could have led to a local increase of volume in stiffening elements such as plates and locally decreasing volumes in rather unnecessary structures or vice versa. In that way total volume could have been almost constant while the stiffness could have been increased (Figure 6). In fact, it seems that CFEs produce concavities in thin rod-like structures which could be compensated for by convexities in other structures such as junctions (Schwen 2010). Thicker trabeculae which are mainly oriented along the main loading axis could over-proportionally benefit from such a thickening. At the same time other structures could have thinned and, thus, compensated the volume change without compensating for the apparent stiffness. These effects require further investigation and maybe an adaption of the CFE construction for structures only a few voxels thick.

The linear models deliver acceptable results at resolutions where other studies (Bevill and Keaveny 2009) suggested the usage of nonlinear FE models. Furthermore acceptable results in comparing simulations to experiments are obtained at resolutions which are coarser than those that can be obtained with state-of-the-art high resolution peripheral quantitative CTs (HRpQCT) (XtremeCT, SCANCO Medical AG, Brüttisellen, Switzerland). Hence, the presented technique allows computing stiffness and strength in combination with a failure load analysis based on linear FE models (Pistoia et al. 2002) at resolutions that are well achievable *in vivo*.

Assessing the influence of additional image processing techniques is beyond the scope of this study. Hence, in order to avoid influences the simulation results, no image denoising (e.g. isotropic, Perona-Malik (Perona and Malik 1990), or anisotropic

(Nemitz et al. 2007) diffusion, or more advanced techniques (Buades et al. 2005)), no more elaborate segmentation algorithms (Pal and Pal 1993; Pham et al. 2000), or joint denoising-segmentation approaches (Mumford and Shah 1989; Chan and Vese 2001) were used. Furthermore, the datasets were coarsened as described in Section 2.1 instead of scanning the samples at different resolutions. This would exclude possible volume losses caused in the scans due to partial volume effects. However, for illustrating the capabilities of CFEs, coarsened datasets were considered sufficient.

The anisotropy and inhomogeneity of the effective elasticity properties of the trabecular bone indicate that the cancellous bone should not be modelled as a homogeneous continuum. The results illustrate that it is necessary to incoroprate the anisotropy of the trabeculuar core using either fabric-based material models or two-scale models.

## 5. Conclusions

Smooth valid µFE-models of vertebral trabecular bone can be generated and efficiently solved using CFEs. Resolutions of 48 µm resolve the microstructure sufficiently. Simulated apparent stiffness of the bone samples delivered an average error of 5.8 % compared to experimental results, for which the computational effort is about one hour on a desktop PC. Coarser models are solved faster and the error in comparison to the experiment considered here is still acceptable at a spatial resolution of 120 µm, despite the fact that the microstructure is not resolved properly anymore. However, the resolution is coarser than those currently achieved with HRpQCTs. Setting up smooth meshes based on the natural voxel grid of the image instead of tetrahedral meshing could be particularly interesting for applications on such CTs in clinical use.

## Acknowledgements

The authors would like to thank the DFG for financial support RU567/8-2 and WI1352/13-1, the Hausdorff Centre for Mathematics at University of Bonn and the ILSB at Vienna University of Technology for providing computational resources, Bettina Willi for suggesting gas micro-pycnometry, Jenny Bienias for performing the gas micro-pycnometry measurements, and Martin Rumpf for valuable advice on CFE and numerical homogenisation.

## References

Arbenz P, van Lenthe G, Mennel U, Müller R, Sala M. 2008. A scalable multi-level preconditioner for matrix-free µ-finite element analysis of human bone structures.

Bern M, Eppstein D. 1992. Ch. Mesh generation and optimal triangulation. In: Computing in Euclidian Geometry. Singapore: World Scientific. pp. 23–90. (Lecture Notes Series on Computing; vol. 1).

Bevill G, Keaveny TM. 2009. Trabecular bone strength predictions using finite element analysis of micro-scale images at limited spatial resolution. Bone 44(4):579 – 584.

Boyd SK, Müller R. 2006. Smooth surface meshing for automated finite element model generation from 3D image data. Journal of Biomechanics 39(7):1287–1295.

Buades A, Coll B, Morel JM. 2005. A review of image denoising algorithms, with a new one. SIAM Journal on Multiscale Modeling and Simulation 4(2):490–530.

Cazzani A, Rovati M. 2003. Extrema of Young's modulus for cubic and transversely isotropic solids. International Journal of Solids and Structures 40(7):1713–1744.

Chan TF, Vese LA. 2001. Active contours without edges. IEEE Transactions on Image Processing 10(2):266–277.

Chevalier Y, Pahr D, Allmer H, Charlebois M, Zysset P. 2007. Validation of a voxel-based FE method for prediction of the uniaxial apparent modulus of human trabecular bone using macroscopic mechanical tests and nanoindentation. Journal of Biomechanics 40(15):3333–3340.

Faulkner KG, Cann CE, Hasegawa BH. 1991. Effect of bone distribution on vertebral strength: assessment with patient-specific nonlinear finite element analysis. Radiology 179:669–674.

Guo XE, Kim CH. 2002. Mechanical consequences of trabecular bone loss and its treatment: a dhree-dimensional model simulation. Bone 30(2):404–411.

Hackbusch W, Sauter SA. 1997a. Composite Finite Elements for the approximation of PDEs on domains with complicated micro-structures. Numerische Mathematik 75(4):447–472.

———. 1997b. Composite Finite Elements for Problems Containing Small Geometric Details. Part II: Implementation and Numerical Results. Computing and Visualization in Science 1(1):15–25.

———. 1998. A New Finite Element Approach for Problems Containing Small Geometric Details. Archivum Mathematicum, Equadiff 9 issue 34(1):105–117.

Hackbusch W. 1994. Iterative Solution of Large Sparse Systems of Equations. Springer (Applied Mathematical Sciences; vol. 95).

He QC, Curnier A. 1995. A more fundamental approach to damaged elastic stress-strain relations. International Journal of Solids and Structures 32(10):1433–1457.

Hengsberger S, Enstroem J, Peyrin F, Zysset PK. 2003. How is the indentation modulus of bone tissue related to its macroscopic elastic response? A validation study. Journal of Biomechanics 36(10):1503 – 1509.

Liehr F, Preusser T, Rumpf M, Sauter S, Schwen LO. 2009. Composite Finite Elements for 3D Image Based Computing. Computing and Visualization in Science 12(4):171–188.

Lin LK. 1989. A concordance correlation coefficient to evaluate reproducibility. Biometrics 45(1):255 – 268.

Morgan EF, Yeh OC, Keaveny TM. 2005. Damage in trabecular bone at small strains. European Journal of Morphology 42(1–2):13–21.

Müller R, Hildebrand T, Rüegsegger P. 1994. Non-invasive bone biopsy: a new method to analyse and display the three-dimensional structure of trabecular bone. Physics in Medicine and Biology 39(1):145–164.

Mumford D, Shah J. 1989. Optimal approximation by piecewise smooth functions and associated variational problems. Communications on Pure and Applied Mathematics 42(5):577–685.

Nemitz O, Rumpf M, Tasdizen T, Whitaker R. 2007. Anisotropic Curvature Motion for Structure Enhancing Smoothing of 3D MR Angiography Data. Journal of Mathematical Imaging and Vision 27(3):217–229.

Oliver W, Pharr G. 1992. An improved technique for determining hardness and elastic modulus using load and displacement sensing indentation experiments. Journal of Materials Research 7(6):1564 – 1583.

Osher S, Sethian JA. 1988. Fronts propagating with curvature dependent speed: Algorithms based on Hamilton–Jacobi formulations. Journal of Computational Physics 79(1):12–49.

Pal NR, Pal SK. 1993. A review on image segmentation techniques. Pattern Recognition 26(9):1277–1294.

Perona P, Malik J. 1990. Scale-Space and Edge Detection Using Anisotropic Diffusion. IEEE Transactions on Pattern Analysis and Machine Intelligence 12(7):629–639.

Pham DL, Xu C, Prince JL. 2000. Current Methods in Image Segmentation. Annual Reviews of Biomedical Engineering 2:315–337.

Pistoia W, van Rietbergen B, Lochmüller EM, Lill CA, Eckstein F, Rüegsegger P. 2002. Estimation of distal radius failure load with micro-finite element analysis models based on three-dimensional peripheral quantitative computed tomography images. Bone 30(6):842 – 848.

R Development Core Team. *R: A Language and Environment for Statistical Computing*. R Foundation for Statistical Computing. Vienna, Austria. ISBN 3-900051-07-0. 2008.

Rho JY, Tsui TY, Pharr GM. 1997. Elastic properties of human cortical and trabecular lamellar bone measured by nanoindentation. Biomaterials 18(20):1325 – 1330.

Ridler TW, Calvard S. 1978. Picture Thresholding Using an Iterative Selection Method. IEEE Transactions on Systems, Man, and Cybernetics 8(8):630–632.

Rumpf M, Schwen LO, Wilke HJ, Wolfram U. 2010. Numerical Homogenization of Trabecular Bone Specimens using Composite Finite Elements. In: *The International Journal of Multiphysics, Special Edition: Multiphysics Simulations – Advanced Methods for Industrial Engineering. Selected Contributions from 1st Fraunhofer Multiphysics Conference*. Fraunhofer. Multi-Science Publishing. pp. 127–143.

Schwen LO. 2010. Composite Finite Elements for Trabecular Bone Microstructures. Ph.D. Dissertation. University of Bonn.

Shewchuk JR. 2002. Delaunay refinement algorithms for triangular mesh generation. Computational Geometry 22(1-3):21–74.

Teng SH, Wong CW. 2000. Unstructured Mesh Generation: Theory, Practice and Applications. International Journal of Computational Geometry and Applications 10(3):227–266.

Thurner PJ, Wyss P, Voide R, Stauber M, Stampanoni M, Sennhauser U, Müller R. 2006. Time-lapsed investigation of three-dimensional failure and damage accumulation in trabecular bone using synchrotron light. Bone 39(2):289–299.

van Rietbergen B, Huiskes R, Eckstein F, Rüegsegger P. 2003. Trabecular Bone Tissue Strains in the Healthy and Osteoporotic Human Femur. Journal of Bone and Mineral Research 18(10):1781–1788.

Verhulp E, van Rietbergen B, Müller R, Huiskes R. 2008. Micro-finite element simulation of trabecular-bone post-yield behaviour – effects of material model, element size and type. Computer Methods in Biomechanics and Biomedical Engineering 11(4):389 – 395.

Wolfram U, Wilke HJ, Zysset PK. 2010. Valid µfinite element models of vertebral trabecular bone can be obtained using tissue properties measured with nanoindentation under wet conditions. Journal of Biomechanics 43(9):1731 – 1737.

———. 2010a. Rehydration of vertebral trabecular bone: Influences on its anisotropy, its stiffness and the indentation work with a view to age, gender and vertebral level. Bone 46(2):348 – 354.

Wolfram U, Schwen LO, Simon U, Rumpf M, Wilke HJ. 2009. Statistical osteoporosis models using composite finite elements: A parameter study. Journal of Biomechanics 42(13):2205–2209.

Woo DG, Won YY, Kim HS, Lim D. 2007. A biomechanical study of osteoporotic vertebral trabecular bone: The use of micro-CT and high-resolution finite element analysis. Journal of Mechanical Science and Technology 21(4):593–601.